*Appl. Math. Mech. -Engl. Ed.*, **39**(1), 1–13 (2018)

**Applied Mathematics and Mechanics (English Edition)**

https://doi.org/10.1007/s10483-018-0000-0

# A Hybrid MDOF Vibration Isolation Platform for Spacecrafts Using the Linear Active Disturbance Rejection Control *

Wei-Chao Chi[1], Shang-Jie Ma[2], Jian-Qiao Sun[2]

1. College of Science and
Key Laboratory of Ministry of Education on Safe Mining of Deep Metal Mines
Northeastern University, Shenyang, 100819, China;
2. Department of Mechanical Engineering
School of Engineering
University of California, Merced, CA 95343, USA

(Received Nov 1, 2019 / Revised )

**Abstract** Hybrid vibration isolation, which takes advantages of both the passive and active approach, has been an important solution for space missions. The objective of this paper is to design a robust, wide bandwidth, multi-degree of freedom vibration isolation platform for payloads on spacecrafts. The proposed solution is based on a parallel mechanism with six VCMs as the actuators. The LADRC algorithm is employed for the active control. Numerical simulation results show that the vibration isolation platform performs effectively over a wide bandwidth, and the resonance introduced by the passive isolation is eliminated. The system robustness to the uncertainties of the structure is also verified by simulation.

**Key words** Hybrid vibration isolation, Stewart platform, Linear active disturbance resistance control, Stability; Robustness

**Chinese Library Classification** CLC number
**2000 Mathematics Subject Classification** MSC number

## 1 Introduction

During the orbital missions of spacecrafts, vibration that caused by several sources such as reaction wheels (RWs), control moment gyroscopes (CMGs), solar array drives and cryo-coolers is always a serious negative impact to the precision payloads. In order to reduce the vibration transmission from the vibration source to the payloads, one of the most intuitive method is to introduce a vibration isolation device in the transmission path to isolate the static instrument from the vibrating structure.

Design of the vibration isolation structure depends on the type and the frequency of the disturbance. As the frequency range of vibration sources covers from low frequency to high frequency, a

* Citation: Chi, Wei-Chao and Ma, Shang-Jie and Sun, Jian-Qiao. A Hybrid MDOF Vibration Isolation Platform for Spacecrafts Using the Linear Active Disturbance Rejection Control. *Applied Mathematics and Mechanics* (*English Edition*) (2018) https://doi.org/10.1007/s10483-018-0000-0

† Corresponding author, E-mail:chiweichao@gmail.com

Project supported by the National Natural Science Foundation of China, the Fundamental Research Funds for the Central Universities and the China Scholarship Council

©Shanghai University and Springer-Verlag GmbH Germany, part of Springer Nature 2018

**Fig. 1** A general Stewart platform.

wide bandwidth of the vibration isolator is demanded. The commonly used passive vibration isolation methods that consists of mass-spring-damper systems work well on high frequency attenuation, but the performance on low frequency is usually limited by the stiffness of the structure, the additional resonance at some specific frequency is also a serious defect. Hybrid isolation that combines passive and active methods was introduced to overcome the defects in passive damping. The active part of the hybrid isolation system can provide real-time force according to the sensor's feedback under certain control law. In the past decade, hybrid vibration isolation has become a practical approach and has been widely used because of the improving performance of microprocessors, actuators and sensors. Cobb *et al.* presented a hybrid isolation struts using LMS control to suppress the vibration in certain broadband [1]. Zhou *et al.* Designed an intelligent vibration isolation which beams with piezoelectric actuators [2]. Zhang *et al.* presented a novel active-passive hybrid vibration control for truss enveloping CMGs on satellites [3].

The isolation structure is the basis of a hybrid vibration isolation system. It supports the payload or connects the payload to the main body, meanwhile plays the role of passive vibration isolation. Many forms of structure have been studied in order to isolate vibration in multiple degree of freedom, in which the Stewart platform is one of the best performing structure for its 6 DOF attitude maneuvering ability [4]. The platform was invented for flight simulating, soon applied to mechanical machining, precision positioning, vibration isolation and many other fields [5]. A Stewart platform consists of six extensible legs with universal joints or spherical joints at each end, connecting the payload-platform to the base-platform as shown in Fig. 1. Fichter [6] and Bonev [7] solved the kinematics problem of a general Stewart platform. Lebert *et al.* presented the dynamic model of Stewart platform using Lagrange method [8]. Xu *et al.* developed a closed-form dynamic model of a Stewart platform and control the platform with PD control [9]. Wu *et al.* proposed a new decoupling condition of stiffness matrix based on elegant algebraic approach to express the dynamic isotropy index of natural frequencies [10].

On the other hand, the controller design is the key issue for the active part of a hybrid vibration isolation system. The control algorithm is used to determine the actuator input by designing the transfer relationship between the system input and feedback signals. [11] and [12] analyzed the various uncertainties in vibration isolation structure and the corresponding mathematical descriptions and designed a robust control system for vibration isolation based on the analysis of uncertainties. At the same time, a big amount of recent research aim at the controlling for systems with uncertainties and inaccurate mathematical model, using nonlinear control and intelligent control algorithms. Active disturbance rejection control (ADRC) [13], fuzzy active control [14], artificial neural network control [15] and genetic algorithm [16] were studied to solve the difficulties of modeling complex systems and nonlinearities. Gao et al gave a method to determine the observer and controller parameters of linear

**Fig. 2** Relationship between generalized and local frames.

active disturbance rejection control (LADRC) by the concept of bandwidth [17]. That made the controller parameters easy to tune, and the physical meaning of the parameters are clearer in practical vibration engineering.

In this paper, a practical approach for designing a hybrid multi-degree of freedom vibration isolation platform is proposed. The contributions of this paper are listed as follows:

1. We extend the LADRC method to the hybrid vibration isolation problem of space parallel structures for the first time, leading to a controller that can reject the disturbances due to external excitations and dynamic couplings of the system.

2. We also report extensive results of the effect of control parameters on vibration isolation bandwidth, present the proof of stability and study the robustness of the control with respect to the modeling error.

The paper is organized as follows. In the second section, the dynamical model of the Stewart platform is established with Newton-Euler Method in task space. In the third section, an LADRC control strategy is presented for the control of MIMO system with parameter uncertainty and external disturbance. In the fourth section, the effectiveness of the approach is verified by numerical simulation.

## 2 Design and modeling of the vibration isolation structure

### 2.1 System configuration and Reference Frames Definitions

The Stewart platform presented in this paper is a general form with six extensible legs connecting the base-platform and the payload-platform. Each leg is equipped with a voice coil motor (VCM) as the actuator. The stator and the mover of the VCM are connected by a piece of diaphragm spring, and the movement is also constrained by a linear bearing to ensure the voice coil moves along the axle. The stator and the mover are treated as the lower and the upper legs together with the other components such as struts, then the lower and the upper legs are connected to the base-platform and the payload-platform by spherical joints at each end.

Define the coordinate frames B and P, which are attached to the base and the payload platforms, and the origins are the mass center of the base and the payload platforms, respectively. The coordinate frames D and U are attached to the lower and upper legs. The relationship between the generalized frame O and the local frame B, P, D, U is shown in Fig. 2.

### 2.2 Dynamic analysis of payload

The position vectors of upper and lower ends of the $i^{th}$ leg in the inertial frame O can be derived from the position vectors of frame P and B as

$$\begin{aligned} \mathbf{t}_{pi} &= \mathbf{t}_p + \mathbf{p}_i \\ \mathbf{t}_{bi} &= \mathbf{t}_b + \mathbf{b}_i \end{aligned} \tag{1}$$

From the subtraction of $\mathbf{t}_{pi}$ and $\mathbf{t}_{bi}$, we can get the vector of the $i^{th}$ leg is

$$\mathbf{l}_i = \mathbf{t}_{pi} - \mathbf{t}_{bi} = (\mathbf{t}_p + \mathbf{p}_i) - (\mathbf{t}_b + \mathbf{b}_i) \tag{2}$$

The velocity of upper and lower ends of the leg can be expressed as

$$\begin{aligned} \dot{\mathbf{t}}_{pi} &= \dot{\mathbf{t}}_p + \omega_p \times \mathbf{p}_i \\ \dot{\mathbf{t}}_{bi} &= \dot{\mathbf{t}}_b + \omega_b \times \mathbf{b}_i \end{aligned} \tag{3}$$

where $\omega_p$, $\omega_b$ are the angular velocity vectors of the payload and the base. Then the velocity of the $i^{th}$ leg is

$$\begin{aligned} \dot{l}_i &= \left(\dot{\mathbf{t}}_{pi} - \dot{\mathbf{t}}_{bi}\right) \cdot \tau_i = \left[\left(\dot{\mathbf{t}}_p + \omega_p \times \mathbf{p}_i\right) - \dot{\mathbf{t}}_b + \omega_b \times \mathbf{b}_i\right] \cdot \tau_i \\ &= \begin{bmatrix} \tau_i^T & (\mathbf{p}_i \times \tau_i)^T \end{bmatrix} \begin{bmatrix} \dot{\mathbf{t}}_p \\ \omega_p \end{bmatrix} - \begin{bmatrix} \tau_i^T & (\mathbf{b}_i \times \tau_i)^T \end{bmatrix} \begin{bmatrix} \dot{\mathbf{t}}_b \\ \omega_b \end{bmatrix} \end{aligned} \tag{4}$$

where $\tau_i = \mathbf{l}_i / l_i$ is the unit vector along the leg. To simplify the matrix form of the length vector, let

$$\begin{aligned} \mathbf{H}_p &= \begin{bmatrix} \tau_1 & \cdots & \tau_6 \\ \mathbf{p}_1 \times \tau_1 & \cdots & \mathbf{p}_6 \times \tau_6 \end{bmatrix}, \\ \mathbf{H}_b &= \begin{bmatrix} \tau_1 & \cdots & \tau_6 \\ \mathbf{b}_1 \times \tau_1 & \cdots & \mathbf{b}_6 \times \tau_6 \end{bmatrix}, \\ \mathbf{x}_p &= \begin{bmatrix} \mathbf{t}_p \\ \theta_p \end{bmatrix}, \ \mathbf{x}_b = \begin{bmatrix} \mathbf{t}_b \\ \theta_b \end{bmatrix} \end{aligned}$$

Equation (4) could be written as

$$\dot{l} = \mathbf{H}_p^T \dot{\mathbf{x}}_p - \mathbf{H}_b^T \dot{\mathbf{x}}_b \tag{5}$$

The force between the upper and the lower legs is

$$\mathbf{F} = -\mathbf{K}(\mathbf{l} - \mathbf{l}_0) - \mathbf{C}\dot{\mathbf{l}} + \mathbf{F}_a \tag{6}$$

where $\mathbf{F} = [F_1, \cdots, F_6]^T$, $\mathbf{l} = [l_1, \cdots, l_6]^T$, $\mathbf{F}_a = [F_{a1}, \cdots, F_{a6}]^T$ is the force vector of the VCMs, $\mathbf{K} = diag\,[k_1, \cdots, k_6]$, $\mathbf{C} = diag\,[c_1, \cdots, c_6]$ are the stiffness and damping matrices of the legs, respectively.

From (5) and (6), the force vector $\mathbf{F}$ can be expressed as

$$\mathbf{F} = -\mathbf{K}\left(\mathbf{H}_p^T \dot{\mathbf{x}}_p - \mathbf{H}_b^T \dot{\mathbf{x}}_b\right) - \mathbf{C}\mathbf{H}_p^T \dot{\mathbf{x}}_p + \mathbf{C}\mathbf{H}_b^T \dot{\mathbf{x}}_b + \mathbf{F}_a \tag{7}$$

The free body diagram of the payload platform is shown in Figure 3. $\mathbf{M}_p$ is the total mass, $\mathbf{F}_w$ and are $\mathbf{M}_w$ external force and torque, respectively. The position vector of the mass center is

$$\mathbf{r} = \mathbf{R}_p \mathbf{r}_0 \tag{8}$$

According to the Newton's dynamical law, the dynamic equation of the payload platform is

$$M_p \mathbf{g} + \mathbf{F}_w + \sum_{i\,=\,1}^{6} \mathbf{F}_{ui} = M_p \mathbf{a}_p \tag{9}$$

where $\mathbf{a}_p$ is the mass center acceleration and

$$\mathbf{a}_p = \ddot{\mathbf{t}}_p + \alpha_p \times \mathbf{r} + \omega_p \times (\omega_p \times \mathbf{r}) \tag{10}$$

**Fig. 3** The force analysis of the top platform.

The balance equation of control force and inertia force according to Euler equation is

$$-\sum_{i=1}^{6}\mathbf{p}_i\times\mathbf{F}_{ui}+\sum_{i=1}^{6}\mathbf{f}_i+M_w+M_p\mathbf{r}\times\mathbf{g}=\mathbf{I}_p^*\alpha_p+\omega_p\times\mathbf{I}_p^*\omega_p \tag{11}$$

where $\mathbf{I}_p^*$ is the moment of translating $\mathbf{I}_p$ to centroid which can be expressed as

$$\mathbf{I}_p^*=\mathbf{I}_p+M_p\left(\mathbf{r}^T\mathbf{r}\mathbf{E}_3-\mathbf{r}\mathbf{r}^T\right) \tag{12}$$

Equations (6), (9) and (11) can be combined into the dynamical equation of system in task-space as

$$\mathbf{J}_p\ddot{\mathbf{x}}_p=\mathbf{J}_b\mathbf{x}_b+\mathbf{H}_p\mathbf{F}-\mathbf{G}+\mathbf{D} \tag{13}$$

where

$$\mathbf{J}_p=\begin{bmatrix} M_p\mathbf{E}_3 & -M_p\tilde{\mathbf{r}} \\ 0 & \mathbf{I}_p^* \end{bmatrix}+\sum_{i=1}^{6}\begin{bmatrix} \mathbf{Q}_{pi} & -\mathbf{Q}_{pi}\tilde{\mathbf{p}}_i \\ -\tilde{\mathbf{p}}_i\mathbf{Q}_{pi} & \tilde{\mathbf{p}}_i\mathbf{Q}_{pi}\tilde{\mathbf{p}} \end{bmatrix},$$

$$\mathbf{J}_b=\sum_{i=1}^{6}\begin{bmatrix} \mathbf{Q}_{pi} & -\mathbf{Q}_{pi}\tilde{\mathbf{p}}_i \\ -\tilde{\mathbf{p}}_i\mathbf{Q}_{pi} & \tilde{\mathbf{p}}_i\mathbf{Q}_{pi}\tilde{\mathbf{p}} \end{bmatrix},$$

$$\mathbf{G}=\begin{bmatrix} -\eta \\ \omega_p\times\mathbf{I}_p^*\omega_p-\sum_{i=1}^{6}\mathbf{f}_i+\sum_{i=1}^{6}\tilde{\mathbf{p}}_i\eta_{6i} \end{bmatrix},$$

$$\mathbf{D}=\begin{bmatrix} \mathbf{F}_{ext} \\ \mathbf{M}_{ext} \end{bmatrix}=\begin{bmatrix} \mathbf{F}_w+M_p\mathbf{g} \\ -\mathbf{M}_w-M_p\mathbf{r}\times\mathbf{g} \end{bmatrix},$$

$$\mathbf{Q}_{pi}=m_{ui}\tau_i\tau_i^T+\frac{\left(\mathbf{E}_3-\tau_i\tau_i^T\right)}{\lambda_i l_i}\left[m_{ui}\kappa_i\left(l_i-l_{ui}\right)+m_{di}l_{di}^2\right]-\frac{1}{\lambda_i l_i}\tilde{\tau}_i\left(\mathbf{I}_{di}+\mathbf{I}_{ui}\right)\tilde{\tau}_i$$

$$\mathbf{Q}_{bi}=\frac{\left(\mathbf{E}_3-\tau_i\tau_i^T\right)}{\lambda_i l_i}[m_{di}l_{di}+m_{ui}\kappa_i l_{ui}]-\frac{1}{\lambda_i l_i}\tilde{\tau}_i\left(\mathbf{I}_{di}+\mathbf{I}_{ui}\right)\tilde{\tau}_i$$

and the calculating sign "~" denotes the transformation of the column vector $\mathbf{x}=[x_1,x_2,x_3]^T$ into

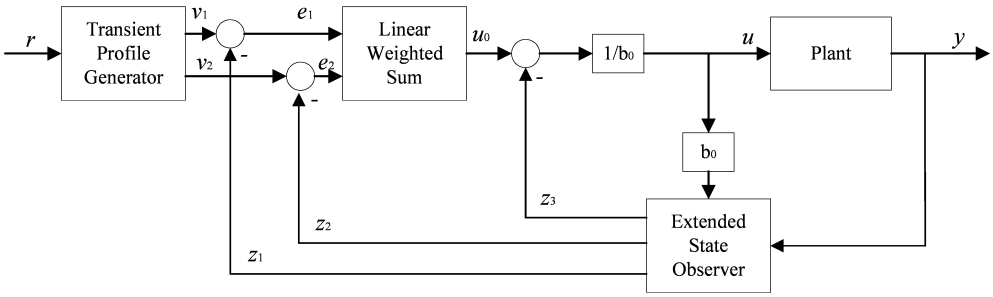


**Fig. 4** The diagram of LADRC

$$\tilde{\mathbf{x}} = \begin{bmatrix} 0 & -x_3 & x_2 \\ x_3 & 0 & -x_1 \\ -x_2 & x_1 & 0 \end{bmatrix} \tag{14}$$

We can obtain the dynamical equation in task-space by substituting Equation (7) into Equation (13) as

$$\begin{aligned} &\mathbf{J}_p\ddot{\mathbf{x}}_p + \mathbf{H}_p\mathbf{C}\mathbf{H}_p^T\dot{\mathbf{x}}_p + \mathbf{H}_p\mathbf{K}\mathbf{H}_p^T\delta x_p = \\ &\mathbf{J}_b\ddot{\mathbf{x}}_b + \mathbf{H}_p\mathbf{K}\mathbf{H}_b^T\delta\mathbf{x}_b + \mathbf{H}_p\mathbf{C}\mathbf{H}_b^T\dot{\mathbf{x}}_b + \mathbf{H}_p\mathbf{F}_a - \mathbf{G} + \mathbf{D} \end{aligned} \tag{15}$$

As shown in Equation (15), the payload platform is a second order plant which is mainly determined by the force from legs, while be disturbed by the motion of the base platform and the external disturbing force.

## 3 LADRC design for MIMO system

### 3.1 The LADRC algorithm

LADRC is the linear form of the ADRC. LADRC augments the states with generalized disturbance, uses the generalized disturbance estimation and the linear feedback to reject the disturbance. It employs the linear extended state observer (LESO) to estimate the dynamic characteristics and the generalized disturbance of the system, then uses the linear combination of the state errors and the generalized disturbance to determine the final control signal. The diagram of LADRC is shown in Fig. 4.

To design a control system for the second order system (15), we consider a general second order SISO system given by

$$\ddot{y} + a_1\dot{y} + a_2 y = b_1\ddot{w} + b_2\dot{w} + b_3 w + bu \tag{16}$$

where $y$, $u$ and $w$ are the output, input and external disturbance of the plant, respectively. The system parameters $a_1$, $a_2$, $b_1$, $b_2$, $b_3$, $b$ are all unknown.

Equation (16) can be written as

$$\ddot{y} = -a_1\dot{y} - a_2 y + b_1\ddot{w} + b_2\dot{w} + b_3 w + (b - b_0)u + b_0 u = f + b_0 u \tag{17}$$

Here, $f = -a_1\dot{y} - a_2 y + b_1\ddot{w} + b_2\dot{w} + b_3 w + (b - b_0)u$ denoted as the generalized disturbance is the key point of the LADRC solution. The internal dynamics $f_1 = -a_1\dot{y} - a_2 y + (b - b_0)u$ and the external disturbance $f_2 = b_1\ddot{w} + b_2\dot{w} + b_3 w$ are together presented in f, which is treated as a new augmented state $x_3 = f$. We then rewrite (17) as

$$\begin{cases} \dot{x}_1 = x_2 \\ \dot{x}_2 = x_3 + b_0 u \\ \dot{x}_3 = h \\ y = x_1 \end{cases} \tag{18}$$

where $x_1 = y$, $x_2 = \dot{x}_1$, $h = \dot{f}$, and $x_3$ is the extended state to be estimated by the observer, $b_0$ is an approximate estimate of $b$ in (16). The state space description of the system is

$$\begin{cases} \dot{\mathbf{x}} = \mathbf{A}\mathbf{x} + \mathbf{B}u + \mathbf{E}h \\ y = \mathbf{C}x \end{cases} \tag{19}$$

where

$$\mathbf{A} = \begin{bmatrix} 0 & 1 & 0 \\ 0 & 0 & 1 \\ 0 & 0 & 0 \end{bmatrix}, \mathbf{B} = \begin{bmatrix} 0 \\ b_0 \\ 0 \end{bmatrix}, \mathbf{C} = [1, 0, 0], \mathbf{E} = \begin{bmatrix} 0 \\ 0 \\ 1 \end{bmatrix} \tag{20}$$

To estimate the states and the generalized disturbance, we use an observer as

$$\begin{cases} e = y - z_1 \\ \dot{z}_1 = z_2 + \beta_1 e \\ \dot{z}_2 = z_3 + \beta_2 e \\ \dot{z}_3 = \beta_3 e \end{cases} \tag{21}$$

where $z_1$, $z_2$, $z_3$ are estimated values of $y$, $\dot{y}$ and $f$, respectively. The observer gain $\beta_1$, $\beta_2$ and $\beta_3$ must be chosen to properly place the eigenvalues of $(\mathbf{A} - \mathbf{LC})$ to make the estimating speed fast and not sensitive to the high frequency noise from the sensors. Gao proposed a method of assigning all the observer eigenvalues at $-\omega_o$ to get optimal estimating performance by simply tuning a single parameter. Equivalently, the gain vector is

$$\mathbf{L} = [\beta_1, \beta_2, \beta_3] = \left[3\omega_o, 3\omega_o^2, \omega_o^3\right] \tag{22}$$

where $\omega_o$ is denoted as the bandwidth of the observer. The observer (21) is known as a Linear Extended State Observer (LESO).

With the LESO, a controller that compensates the generalized disturbance can be designed by the feedback linearization method as

$$u = \frac{-z_3 + u_0}{b_0} \tag{23}$$

where $u_0$ is the error feedback variable which is a new input to be determined. Substitute the controller (23) into the system (18), we can get

$$\ddot{y} = (f - z_3) + u_0 = \bar{e}_3 + u_0 \tag{24}$$

where $\bar{e}_3$ is the estimation error in $z_3$. For an ideal observer, we can ignore the estimation error then we obtain a simple linear double-integrator relationship between the output and the new input $u_0$ as

$$\ddot{y} \approx u_0 \tag{25}$$

Hence, the generalized disturbance is estimated and offset, that is to say the disturbance and the uncertainties involved in generalized disturbance do not need to be mathematically detailed. To design a tracking controller for this double-integrator relation, select the new input $u_0$ as

$$u_0 = k_p(r - z_1) - k_d z_2 \tag{26}$$

where $r$ is the reference input. This form of PD controller makes the closed-loop transfer function pure second order without a zero, and to place all closed-loop poles at $-\omega_o$ which denotes as the control bandwidth, choose the PD parameters as

$$k_d = 2\xi\omega_c,\ k_p = \omega_c^2 \tag{27}$$

where $\xi$ is the damping ratio for reducing oscillation. Then the objective can make the system output $y$ behave as the reference signal by the manipulative variable $u$ as

$$u = -\frac{k_p}{b_0} z_1 - \frac{k_d}{b_0} z_2 - \frac{1}{b_0} z_3 + \frac{k_p}{b_0} r \tag{28}$$

### 3.2 Discussion of the stability

As discussed above, LADRC is a combination of linear estimator and linear feedback controller, so the stability can be proved in accordance with the Separation Principle under some assumptions.

#### 3.2.1 Convergence of the LESO

Let $e_i = x_i - z_i, i = 1, 2, 3$. From Equations (18) and (21), the observer error can be expressed as

$$\begin{cases} \dot{e}_1 = e_2 - \beta_1 e_1 \\ \dot{e}_2 = e_3 - \beta_2 e_1 \\ \dot{e}_3 = -\beta_3 e_1 + h \end{cases} \tag{29}$$

Rewrite Equation (29) as

$$\dot{\mathbf{e}} = \mathbf{A}_e \mathbf{e} + \mathbf{E}h \tag{30}$$

where

$$A_e = \begin{bmatrix} -\beta_1 & 1 & 0 \\ -\beta_2 & 0 & 1 \\ -\beta_3 & 0 & 0 \end{bmatrix}, E = \begin{bmatrix} 0 \\ 0 \\ 1 \end{bmatrix} \tag{31}$$

For the chosen observer gain $\mathbf{L} = [\beta_1, \beta_2, \beta_3] = \left[3\omega_o, 3\omega_o^2, \omega_o^3\right]$, the matrix $\mathbf{A}$ is stable. For any $h$ which is bounded, Equation (30) is bounded, so the LESO is bounded-input bounded-output (BIBO) stable.

#### 3.2.2 Convergence of the LADRC

Theorem 3.1: If $h = \dot{f}$ is bounded, the observer (21) and the control strategy for the double integrator (23) are stable, then the combined observer and feedback is stable.

The closed-loop system presented in Equations (19)-(28) can be expressed in the state-space form as

$$\begin{bmatrix} \dot{\mathbf{X}} \\ \dot{\mathbf{Z}} \end{bmatrix} = \begin{bmatrix} \mathbf{A} & -\frac{1}{b_0}\mathbf{BK} \\ \mathbf{LC} & \mathbf{A} - \mathbf{LC} + \frac{1}{b_0}\mathbf{K} \end{bmatrix} \begin{bmatrix} \mathbf{X} \\ \mathbf{Z} \end{bmatrix} + \mathbf{H} \begin{bmatrix} r \\ h \end{bmatrix} \tag{32}$$

where matrices $\mathbf{A}, \mathbf{B}, \mathbf{C}$ are presented in Equation (20), $\mathbf{K} = [k_p, k_d, 1]$, matrix $\mathbf{H}$ is

$$\mathbf{H} = \begin{bmatrix} 0 & k_p & 0 & 0 & 0 & 0 \\ 0 & 0 & 1 & 0 & k_p & 0 \end{bmatrix}^T \tag{33}$$

The eigenvalues of system (32) is

$$eig\left(\begin{bmatrix} \mathbf{A} & -\frac{1}{b_0}\mathbf{BK} \\ \mathbf{LC} & \mathbf{A} - \mathbf{LC} + \frac{1}{b_0}\mathbf{BK} \end{bmatrix}\right) = eig\left(\begin{bmatrix} \mathbf{A} - \frac{1}{b_0}\mathbf{BK} & -\frac{1}{b_0}\mathbf{BK} \\ \mathbf{0} & \mathbf{A} - \mathbf{LC} \end{bmatrix}\right) \tag{34}$$

It is easy to verify that all the eigenvalues of $\mathbf{A} - \frac{1}{b_0}\mathbf{BK}$ and $\mathbf{A} - \mathbf{LC}$ have negative real part. For any $r$ and $h$ which are bounded, Equation (34) is bounded. Therefore the LADRC is BIBO stable.

### 3.3 MIMO Decoupling Control

Consider the MIMO systems (15) in the following form

$$\begin{cases} \ddot{\mathbf{x}} = \mathbf{f}\left(x, \dot{x}, w, \dot{w}, t\right) + \mathbf{Bu} \\ \mathbf{y} = \mathbf{x} \end{cases} \tag{35}$$

where $\mathbf{x} = [x_1, x_2, \cdots, x_6]^T$, $\mathbf{f} = [f_1, f_2, \cdots, f_6]^T$, $\mathbf{u} = [u_1, u_2, \cdots, u_6]^T$. If the control matrix

$$\mathbf{B} = \begin{bmatrix} b_{11} & \cdots & b_{16} \\ \vdots & \vdots & \vdots \\ b_{61} & \cdots & b_{66} \end{bmatrix} = \mathbf{J}_p^{-1}\mathbf{H}_p \tag{36}$$

is reversible, introducing the virtual control matrix $\mathbf{U} = \mathbf{Bu}$, the input/output relationship of the $i^{th}$ channel is

$$\begin{cases} \ddot{x}_i = f_i\left(x, \dot{x}, \cdots, x_6, \dot{x}_6, t\right) + U_i \\ y_i = x_i \end{cases} \tag{37}$$

**Fig. 5** The diagram of LADRC for a MIMO system.

**Table 1** Main parameters of the platform.

| Parameter | Value |
|---|---|
| Mass of upper platform | 8.14kg |
| Moment of Inertia of top platform | $\text{diag}(4.1, 4.4, 8) \times 10^{-2} kg \cdot m^2$ |
| Moment of Inertia of upper leg | $\text{diag}(1.895, 103, 103) \times 10^{-5} kg \cdot m^2$ |
| Moment of Inertia of lower leg | $\text{diag}(9.63, 154, 154) \times 10^{-4} kg \cdot m^2$ |
| Mass of each upper leg | $0.0793kg$ |
| Mass of each lower leg | $1.16kg$ |
| Stiffness of diaphragm spring | $4.8 \times 10^4 N/m$ |

Then, the virtual control variable $Ui$ of each channel and the system output $y_i$ are in a SISO relationship, that is, $U_i$ and $y_i$ are completely decoupled. The external disturbance and the coupling between different actuators are canceled together as the generalized disturbance by LADRC. Decoupling control can be realized by embedding six LADRC in parallel between control vector $\mathbf{U}$ and output $\mathbf{y}$. The actual control vector $\mathbf{u}$ can be determined by the virtual control vector $\mathbf{U}$ as Fig. 5

$$\mathbf{u} = \mathbf{B}^{-1}\mathbf{U} \tag{38}$$

Here the perturbation of matrix $\mathbf{B}$ can be rejected in LADRC of each channel, so the accurate model of $\mathbf{B}$ is not necessary to be known. This will be verified in the simulation.

## 4 Numerical Simulation studies

In this section, the model of the 6-DOF vibration isolation system has been developed using the Matlab and Simulink software to demonstrate the efficiency of the LADRC approach. The parameters for the platform are listed in Table 1. The results of the vibration isolation simulation are presented later.

### 4.1 Frequency response of the system

To investigate the bandwidth of the vibration isolation system, we linearize the open-loop and closed-loop model with the disturbance vector $\mathbf{w}$ and output vector $\mathbf{y}$ as the system input and output. The open-loop model represents the passive vibration isolation structure, while in contrast the closed-loop model represents the hybrid vibration isolation system with active control force. To simplify the diagram, the frequency response of displacement from the base platform to the payload platform along x-axis is presented. The other input-output combinations response similarly, with slight differences on

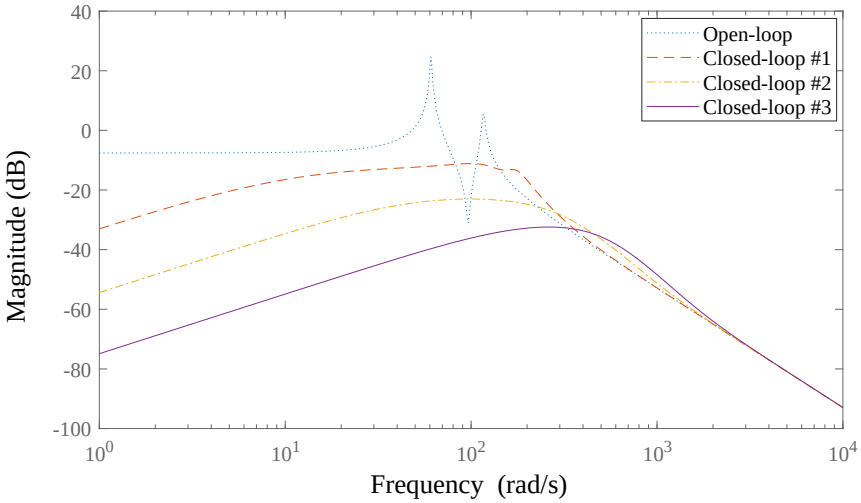


**Fig. 6** The frequency response from the base to the payload

resonance frequency and response magnitude.

From the open-loop frequency response shown by the blue curve in Fig. 6, the response of the passive part of the vibration isolation platform has two resonance peaks at 60.6rad/s and 116.0rad/s. The open-loop transmission ratio reach to 24.6dB. That is to say the passive structure is a lowpass system which can attenuate the vibration in high frequency band while the vibration of low frequency passes through the isolation platform completely. The resonance frequencies vary between the different inputs and outputs.

The tuning of control parameters is based on the frequency response of the structure. The two parameters, observer bandwidth $\omega_o$ and controller bandwidth $\omega_c$ are gradually increased from the second nature frequency. The closed-loop frequency response is shown in Fig. 6, where the red curve represents the vibration transmission ratio with the parameters $\omega_o = 100$, $\omega_c = 100$ while the orange and purple curves represent that with the parameters $\omega_o = 500$, $\omega_c = 100$ and $\omega_o = 500$, $\omega_c = 500$, respectively. The control signal $u$ for each actuator is limited to $[-50, 50]$ in order to make the system realistic. It is shown that under LADRC, the vibration amplification at frequency lower than 300rad/s is attenuated significantly while the vibration amplification at high frequency performs as well as that under passive isolation. At the same time, the resonant peaks of open-loop response disappear in response.

The relation between the parameters and the vibration transmissibility is also clear from Fig. 6. The parameters $\omega_o$ and $\omega_c$, which decide the position of closed-loop poles, affect the maneuvering speed and reflect in the bandwidth of the active vibration isolation. The observer bandwidth and the controller bandwidth should cover the bandwidth that the vibration is amplified by the structure.

### 4.2 Time-domain response

Vibration simulations for the system with passive vibration isolation structure and active control are respectively tested at fixed frequencies. It is assumed that the displacement and attitude measurements in the inertial frame are obtained by MEMS sensors and certain multi-sensors fusion algorithm. The initial value of all the states is set to be 0, and the sample rate is set to be 2000Hz.

The first case presented the fixed-frequency sinusoidal vibration tests. The displacement amplitude of excitation is given as $10^{-4}$m at the resonance frequency of 60.6rad/s. It can be seen from Fig. 7 that under the parameters $\omega_o = 500$, $\omega_c = 500$ , and the system response is attenuated to 1/1000 of the open-loop response by the active control. The other outputs response similarly with different attenuating range.

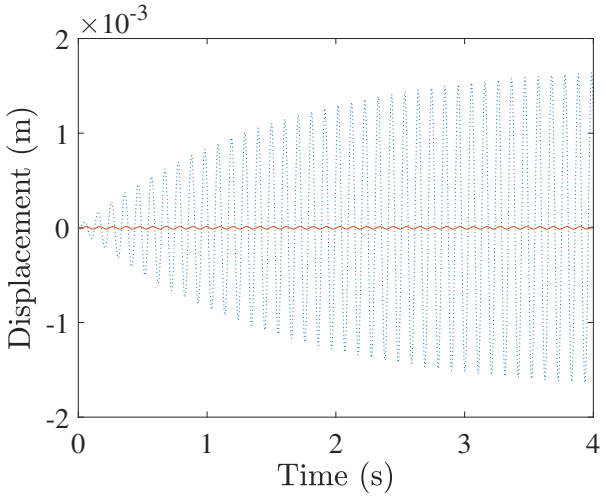


**Fig. 7** The response of sinusoidal disturbance.

The second case presented the shock test. At time $t = 0.1$s, we imposed a pulse signal with the amplitude of $10^{-3}$m and the width of 0.001s as the shock disturbance. From Figure 8, the active control can lead to a fast convergence, the time to reach steady state is reduced from 3s to 0.05s, and the system response is attenuated to 1/10 of the open-loop response. The other outputs response in the same trend with different attenuating range.

The simulation results of the time response show that the higher controller and observer bandwidth made output response faster, which results in better attenuation of the disturbance and shorter adjustment time when applied in vibration isolation system. On the other hand, the higher observer bandwidth will make the system more sensitive to the high frequency noise in practical applications. As a conclusion, the optimal control parameters are not obtained by the biggest bandwidth, but should be tuned in a compromise between vibration attenuation and noise sensitivity according to the actual working conditions in practical engineering.

### 4.3 Robustness to the modeling error

Considering the parameters in the control loop, the matrix $\mathbf{B}^{-1}$ in Equation (38) is the only variable that contains the information of the controlled plant. To investigate the robustness of the system, we change the structure parameters contained in $\mathbf{B}$ drastically while keep the control parameters constant. The frequency response is analyzed with setting the mass and moment of inertia of the payload platform to 0.2 and 5 times of their original value.

As shown in Fig. 9, the modeling errors in matrix $\mathbf{B}$ slightly affect the frequency response of the upper platform of the vibration isolation system. The response amplitude of the output becomes only slightly larger as the mass and moment of inertia is estimated 5 times of the actual value. The proposed vibration isolation system performs very robust to the modeling errors, which can be considered as detailed mathematical model independent.

## 5 Conclusions

A practical approach to the 6 DOF vibration isolation system for payloads on spacecraft by using Linear Active Disturbance Rejection Control is proposed in this paper. By analyzing the dynamic model of the employed Stewart platform, the order of the control plant is determined. A control solution is then presented based on LADRC strategy which is mathematical model independent, and the system parameters are tuned according to the operating bandwidth. The simulation results show that with the properly tuned LADRC parameters, the vibration isolation system can attenuate the transmission of vibration for about 30dB in low frequency and eliminate the resonance at nature

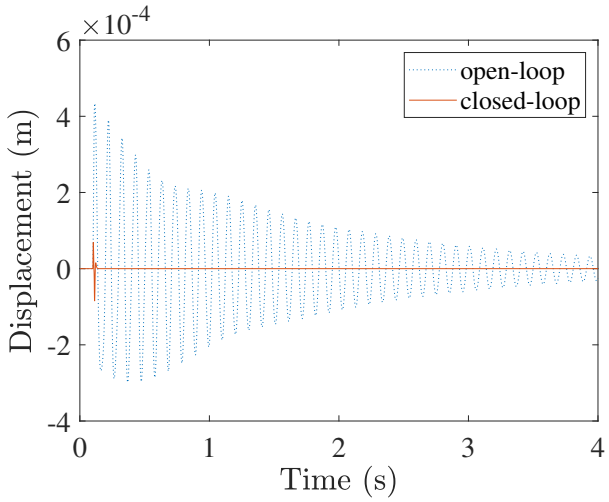


**Fig. 8** The response of shock disturbance.

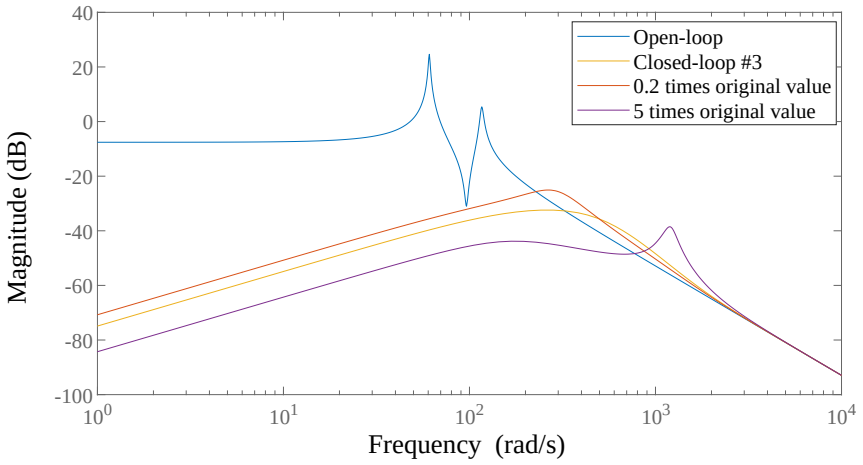


**Fig. 9** The frequency response from the base to the payload with modeling error

frequency effectively, while it performs as well as passive isolation in high frequency. Furthermore, the robustness of the control system with respect to the modeling error is also verified by drastically changing the parameters of the model.

## Acknowledgement

This work was supported by the National Natural Science Foundation of China through the Grants (11572215). The first author gratefully acknowledges the support of the Fundamental Research Funds for the Central Universities (N160503002) and China Scholarship Council (CSC).

## References

[1] Cobb RG, Sullivan JM, Das A, Davis LP, Hyde TT, Davis T, Rahman ZH, Spanos JT (1999) Vibration isolation and suppression system for precision payloads in space. *Smart Materials and Structures* **8**(6), 798

[2] Zhou WY, Li DX (2012) Design and analysis of an intelligent vibration isolation platform for reaction/momentum wheel assemblies. *Journal of Sound and Vibration* **331**(13), 2984–3005

[3] Zhang Y, Zang Y, Li M, Wang Y, Li W (2017) Active-passive integrated vibration control for control moment gyros and its application to satellites. *Journal of Sound and Vibration* **394**, 1–14

[4] Stewart D (1965) A platform with six degrees of freedom. *Proceedings of the institution of mechanical engineers* **180**(1), 371–386

[5] Furqan M, Suhaib M, Ahmad N (2017) Studies on stewart platform manipulator: A review. *Journal of Mechanical Science and Technology* **31**(9), 4459–4470

[6] Fichter EF (1986) A stewart platform-based manipulator: general theory and practical construction. *The International Journal of Robotics Research* **5**(2), 157–182

[7] Bonev IA, Ryu J (2000) A new method for solving the direct kinematics of general 6-6 stewart platforms using three linear extra sensors. *Mechanism and Machine Theory* **35**(3), 423–436

[8] Lebret G, Liu K, Lewis FL (1993) Dynamic analysis and control of a stewart platform manipulator. *Journal of Robotic systems* **10**(5), 629–655

[9] Xu P, Wang D (2005) Vibration damping modeling of stewart platform through newton-euler approach. In: *Proceedings of Smart structures and materials 2005: smart structures and integrated systems*, vol 5764, pp 650–661

[10] Wu Y, Yu K, Jiao J, Cao D, Chi W, Tang J (2018) Dynamic isotropy design and analysis of a six-dof active micro-vibration isolation manipulator on satellites. *Robotics and Computer-Integrated Manufacturing* **49**, 408–425

[11] Gspr P, Szszi I, Bokor J (2002) Robust control design for mechanical systems using the mixed synthesis. *Periodica Polytechnica Transportation Engineering* **30**(1-2), 37–52

[12] Zhang X, Shao C, Li S, Xu D, Erdman A (2001) Robust h vibration control for flexible linkage mechanism systems with piezoelectric sensors and actuators. *Journal of Sound and Vibration* **243**(1), 145–155

[13] Han JQ (2009) From pid to active disturbance rejection control. *IEEE Transactions on Industrial Electronics* **56**(3), 900–906

[14] Zeinoun IJ, Khorrami F (1994) An adaptive control scheme based on fuzzy logic and its application to smart structures. *Smart Materials and Structures* **3**(3), 266

[15] Ghaboussi J, Joghataie A (1995) Active control of structures using neural networks. *Journal of Engineering Mechanics* **121**(4), 555–567

[16] Curtis AR (1991) An application of genetic algorithms to active vibration control. *Journal of Intelligent Material Systems and Structures* **2**(4), 472–481

[17] Gao Z (2006) Scaling and bandwidth-parameterization based controller tuning. In: *Proceedings of Proceedings of the American control conference*, vol 6, pp 4989–4996